journal

J. Am. Ceram. Soc., **80** [12] 3157–71 (1997)

Nanocrystalline Titanium Oxide Electrodes for Photovoltaic Applications

Christophe J. Barbé,* Francine Arendse, Pascal Comte, Marie Jirousek, Frank Lenzmann,
Valery Shklover, and Michael Grätzel

Institute of Physical Chemistry, Swiss Federal Institute of Technology, Lausanne, Switzerland

During the past five years, we have developed in our laboratory a new type of solar cell that is based on a photoelectrochemical process. The light absorption is performed by a monolayer of dye (i.e., a Ruthenium complex) that is adsorbed chemically at the surface of a semiconductor (i.e., titanium oxide (TiO_2)). When excited by a photon, the dye has the ability to transfer an electron to the semiconductor. The electric field that is inside the material allows extraction of the electron, and the positive charge is transferred from the dye to a redox mediator that is present in solution. A respectable photovoltaic efficiency (i.e., 10%) is obtained by the use of mesoporous, nanostructured films of anatase particles. We will show how the TiO_2 electrode microstructure influences the photovoltaic response of the cell. More specifically, we will focus on how processing parameters such as precursor chemistry, temperature for hydrothermal growth, binder addition, and sintering conditions influence the film porosity, pore-size distribution, light scattering, and electron percolation and consequently affect the solar-cell efficiency.

I. Introduction

Recently, nanocrystalline materials have attracted an increasing amount of attention in the scientific community because of their spectacular physical and chemical properties. These unusual properties result from the ultrafine structure (i.e., a grain size of <50 nm) of these materials and can be classified in two categories: properties that are relative to the bulk and properties that are relative to the surface. More precisely, their small crystallite size can lead to quantum confinement effects in semiconductors[1] (silicon or cadmium sulfide, CdS), magnetic materials with monodomain grains that have been used for high-density information storage and magnetic refrigeration,[2] or materials with strong piezoelectric properties.[1,3] Another characteristic of these materials is their high grain-boundary-to-volume ratio, which enables the fabrication of ductile[4] or superplastic ceramics[5] and the low-temperature synthesis of ultradense materials or coatings and highly porous membranes[6] and electrodes.[7]

By using this very high surface area, which is provided by the nanocrystalline particles, we have successfully developed in our laboratory a new type of solar cell that is based on a photoelectrochemical process.[8,9] In contrast to conventional solar cells, the light-absorption and charge-separation steps are differentiated. The light absorption is performed by a monolayer of dye (i.e., a Ruthenium complex) that is adsorbed chemically at the surface of a semiconductor (i.e., titanium oxide (TiO_2)). Via absorption of a photon (excitation), the dye changes from the electronic ground state (S^0) to the excited state (S^*). Then, it injects an excited electron into the conduction band of the semiconductor (TiO_2) and, thus, becomes oxidized (S^+). The recombination of the electron in the conduction band and the hole on the oxidized dye is much slower than the reduction from the S^+ state by the reduced state of the mediator that is in solution. Thus, charge separation is efficient. Next, the oxidized mediator is reduced at the counter electrode. The maximum voltage corresponds to the difference between the redox potential of the mediator and the Fermi level of the semiconductor. The simplicity of the cell design, as well as its respectable efficiency (i.e., 10%–11%), promises a significant cost reduction of solar energy.

This respectable photovoltaic efficiency is obtained via the use of porous nanostructured films that are synthesized by tape casting nanocrystalline anatase particles. In the following, we will describe how the TiO_2 electrode microstructure—and, thus, colloidal synthesis and film processing—influences the photovoltaic response of the cell. More precisely, we will investigate the relationships between the particle size, the surface area, the dye adsorption, and the electron injection in the semiconductor. We also will show how the initial particle-size distribution influences the pore-size distribution in the film, which, in turn, affects the electrolyte transport phenomena and, therefore, the internal resistance of the cell, as well as its global efficiency.

II. Experimental Procedure

(1) Colloidal Synthesis

Typical synthesis of the TiO_2 nanoparticles can be described as follows. A quantity (125 mL) of titanium isopropoxide (97%, Aldrich Chemical Co., Milwaukee, WI) is added, dropwise and at room temperature, to 750 mL of a 0.1*M* nitric acid solution under vigorous stirring. A white precipitate forms instantaneously. Immediately after the hydrolysis, the slurry is heated to 80°C and stirred vigorously for 8 h, to achieve peptization (i.e., destruction of the agglomerates and redispersion into primary particles). The solution is then filtered on a glass frit to remove nonpeptized agglomerates. Water is added to the filtrate to adjust the final solids concentration to ~5 wt%.

The growth of these particles, up to 10–25 nm, is achieved under hydrothermal conditions in a titanium autoclave that is heated for 12 h in the temperature range of 200°–250°C; the temperature is dependent on the desired particle size. Sedimentation occurs during the autoclaving, and the particles are redispersed using a titanium ultrasonic horn (400 W, 15 × 2 s pulses). After two sonications, the colloidal suspension is introduced in a rotary evaporator and evaporated (35°C, 30 mbar (3 MPa)) to a final TiO_2 concentration of 11 wt%.

Several variations of this synthesis were designed, to study the influence of processing parameters, such as precipitation pH, hydrolysis rate, autoclaving pH, and precursor chemistry, on the morphology of the final particles. To study the influence of pH and the hydrolysis rate during precipitation, titanium alkoxide was added using different speeds (varying from one shot to dropwise) to an acidic (0.1*M* nitric acid), neutral, and basic (0.1*M* ammonia) water solution. To study the influence of

---

C. J. Brinker—contributing editor

Manuscript No. 191723. Received June 24, 1996; approved March 31, 1997.
Supported by the Swiss National Science Foundation and the Institut für Angewandte Photovoltaik (Gelsenkirschen, Germany).

*Member, American Ceramic Society.

pH during hydrothermal growth, precipitates were peptized and autoclaved at a temperature of 250°C in different environments: at pH 1 in nitric acid, at pH 11 in ammonia, and at pH 13 in a triethylamine solution. The influence of the titanium precursor chemistry was studied by substituting titanium ethoxide or titanium butoxide (both purchased from Fluka Chemical Corp., Ronkonkoma, NY) for titanium isopropoxide or by prereacting the titanium alkoxide with acetic acid or acetyl acetone in a moisture-free environment (i.e., an argon-gas glove box) prior to hydrolysis.[10]

(2) *TiO_2 Electrode Preparation*

The TiO_2 paste is deposited using a simple doctor-blade technique on sheet glass (Nippon Sheet Glass, Hyogo, Japan) that has been coated with a fluorine-doped stannic oxide (SnO_2) layer (sheet resistance of 8–10 Ω/□). The resulting green layer is ~100 μm thick. The layer is dried in air at room temperature for 10 min, followed by treatment at a temperature of ~50°C for 15 min. Then, the film is heated to 450°C at a rate of 20°–50°C/min and left at 450°C for 30 min before cooling to room temperature.

To prevent cracking during film drying, which thus renders the synthesis of sintered films that are 10 μm thick possible, polyethylene glycol (PEG, molecular weight (MW) of 20000, Merck, Darmstadt, Germany) is added in a proportion of 0%–50% of the TiO_2 weight. The resulting paste is stored in a screw-threaded glass bottle until deposition.

An additional step can be performed on the fired electrode. This step consists of impregnating the TiO_2 film with a solution of titanium tetrachloride ($TiCl_4$) that has been dissolved in ice water (concentration of 0.1*M*), which is followed by a firing at 450°C for 30 min.

(3) *Colloids and Electrodes Characterization*

The particle-size distribution was studied using photon correlation spectroscopy (Model BI2030AT instrument (Brookhaven Instruments, Austin, TX) that was equipped with a 488 nm laser) and centrifugal sedimentation (Model Capa 700, Horiba, Tokyo, Japan).† The surface area of the colloids was determined using a nitrogen adsorption apparatus (Model Gemini 2327, Micromeretics Instrument Corp., Norcross, GA). Zeta potential studies on different suspensions were performed (Model Zetasizer, Malvern Instruments, Malvern, U.K.). Additional characterization included transmission electron microscopy (TEM), which was performed using a high-resolution microscope (Model CM30ST, Philips Research Laboratories, Eindhoven, The Netherlands), and X-ray diffractometry (XRD), which was performed using a powder diffractometer (Scintag, Santa Clara, CA) using Cu*K*α radiation.

The electrode microstructure was studied using a high-resolution scanning electron microscopy (SEM) field-emission microscope (Model S-900, Hitachi, Tokyo, Japan). The electrode pore-size distribution was studied using a nitrogen adsorption–desorption apparatus (Model ASAP 2010, Micromeretics Instrument Corp.). The optical transmissions and reflections of the TiO_2 films were recorded in the wavelength range of 300–800 nm on an ultraviolet–visible light (UV–VIS) spectrometer (Varian, Palo Alto, CA) that was equipped with an integrating sphere.

(4) *Solar-Cell Assembly*

The TiO_2 nanocrystalline electrode was immersed overnight in a solution of ruthenium dye (ruthenium (2,2′bipyridyl-4,4′-dicarboxilate)$_2$ (NCS)$_2$ that was dissolved in ethanol) (concentration of $3 \times 10^{-4}M$). The electrode was then rinsed with acetonitrile and dried. One drop of an iodine-based electrolyte solution was deposited onto the surface of the electrode and penetrated inside the TiO_2 film via capillary action. The electrolyte solution was composed of 0.5 mmol/L of homemade dimethyl hexyl imidazolium,[11] 20 mmol/L of iodine (I_2), 40 mmol/L of lithium iodide (LiI), and 500 mmol/L of *tert*-butyl pyridine that was dissolved in acetonitrile (all the chemicals were purchased from Fluka Chemical). A platinized counter electrode was then clipped onto the top of the TiO_2 working electrode to form our test cell.

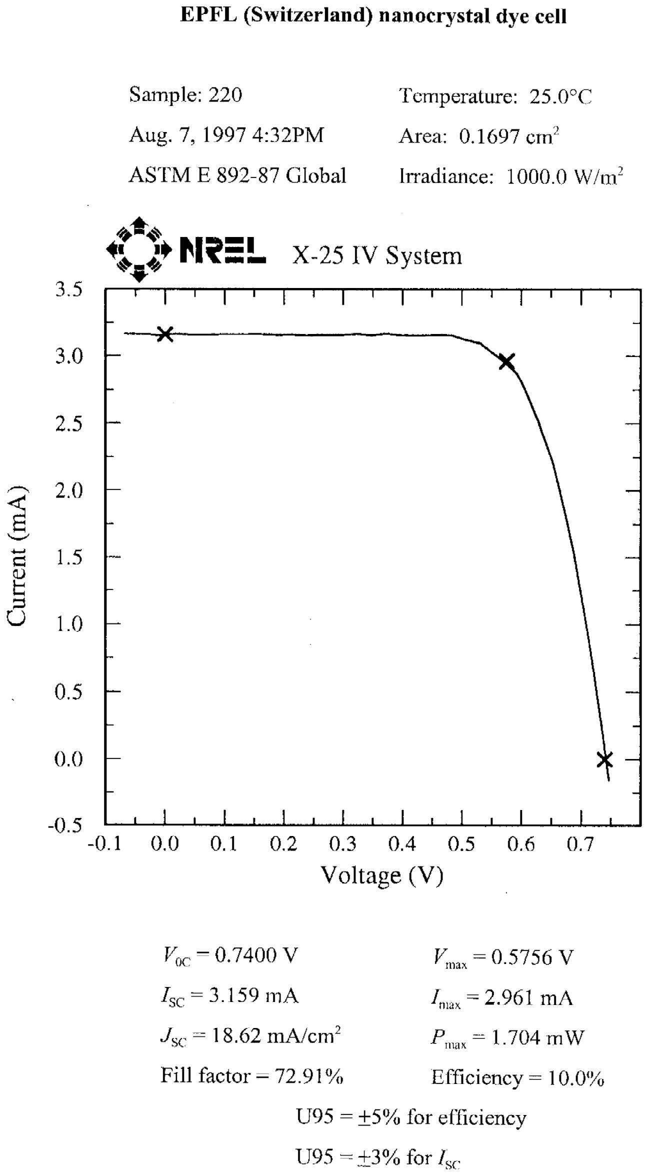

Fig. 1. Typical graph of current versus voltage for our dye-sensitized solar cell. The photocurrent that has been measured under 100 mW/cm^2 of simulated solar light (AM 1.5, which corresponds to a solar elevation of 42° to the horizon) and the open-circuit voltage are equivalent to 18.6 mA/cm^2 and 0.74 V, respectively; the fill factor is 0.73 and the efficiency is 10%.

(5) *Photovoltaic Characterizations*

The photovoltaic properties of the solar cells were characterized using two different techniques. The first technique consisted of recording the current–voltage characteristics of the solar cell in the dark and under an illumination of AM 1.5 (or 1 Sun), which corresponded to a solar elevation of 42° to the

Table I. Surface Area and Average Particle Size of Samples Autoclaved at Different Temperatures

Powder	Surface area (m^2/g)	d_{BET}† (nm)
Autoclaved at 200°C	145	10.8
Autoclaved at 210°C	130	12.0
Autoclaved at 230°C	115	13.6
Autoclaved at 250°C	108	14.5
P25 (Degussa)	55	28.4

†Average diameter back-calculated from the surface area, assuming that the particles are spherical.

---

†Not corrected for light scattering.

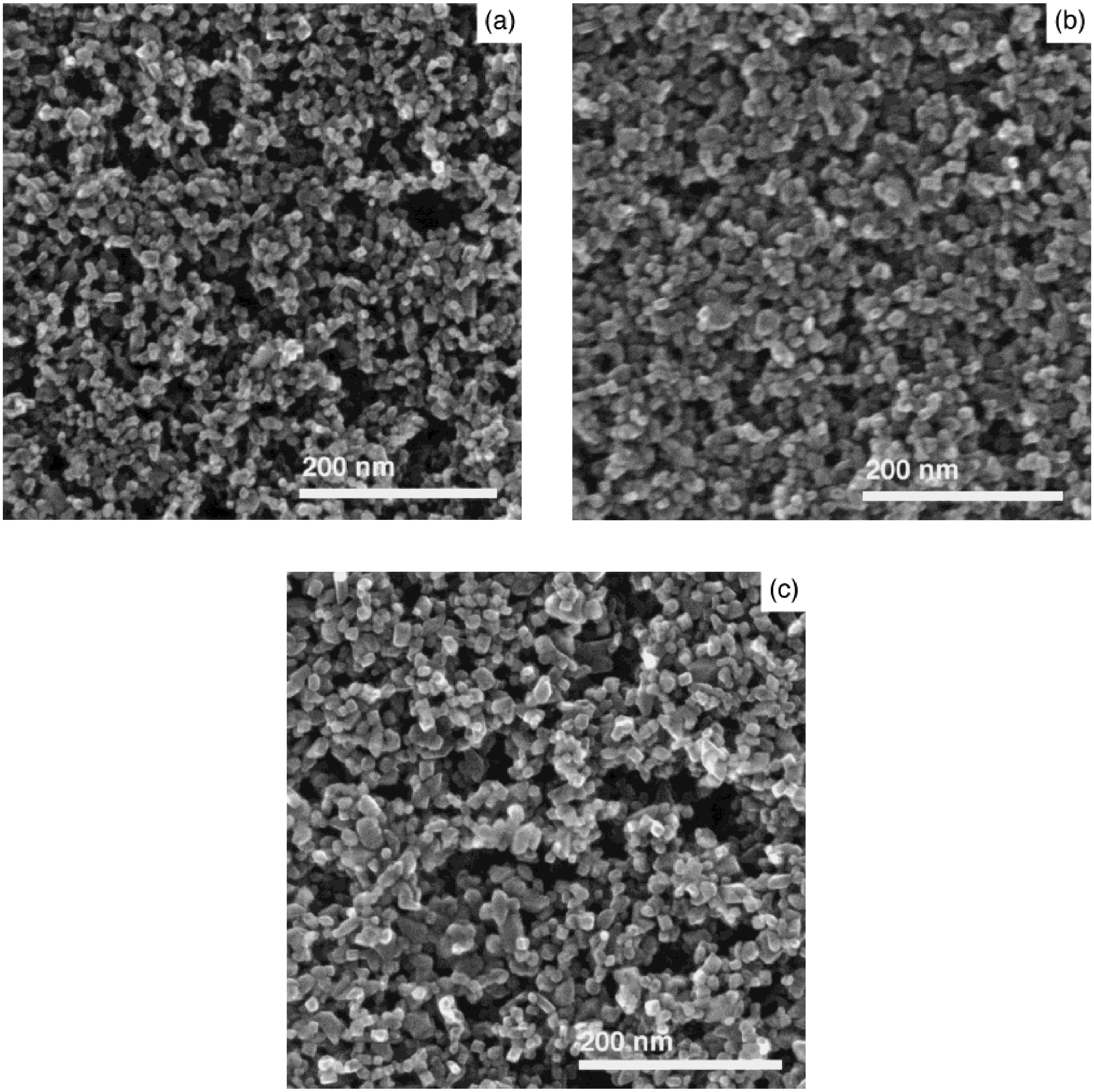

Fig. 2. SEM micrographs of films synthesized from colloids autoclaved at (a) 210°, (b) 230°, and (c) 250°C.

horizon. An additional measurement was performed at a lower light intensity (1/10 Sun) to examine the potential nonlinearity in the cell response. A typical current–voltage curve is shown in Fig. 1. This curve can be described using the following set of parameters: the short-circuit current (I_{SC}), in units of mA/cm^2), the open circuit voltage (V_{0C}, in units of mV/cm^2), the efficiency percentage (η), and the fill factor percentage (FF). I_{SC} is the current that is recorded when the voltage is zero, and V_{0C} is the potential when the current is zero. So as not to overwhelm the reader with current–voltage curves, the performances of the cells will be discussed using the previously described set of parameters. The efficiency is given by the ratio of the electrical power that is delivered by the cell divided by the power of the light that is illuminating the cell.

The second type of photovoltaic test that has been performed on the solar cell is called incident photon conversion efficiency (IPCE). It represents the percentage of incident photons that are converted to electrons at a certain wavelength and is defined by the formula

$$\mathrm{IPCE}(\lambda) = 1240\left(\frac{I_{SC}}{\lambda\Phi}\right) \tag{1}$$

where λ is the wavelength (in nanometers) and Φ is the incident radiative flux (in units of W/m^2). The experimental details that concern the two experimental setups that are used for these characterizations are given elsewhere.[12]

III. Results and Discussion

(1) Influence of Processing Parameters on the Final Film Microstructure

(A) Influence of Hydrolysis pH and Rate: No noticeable difference, with respect to the Brunauer–Emmett–Teller (BET) surface area, is observed in the precipitates, regardless of

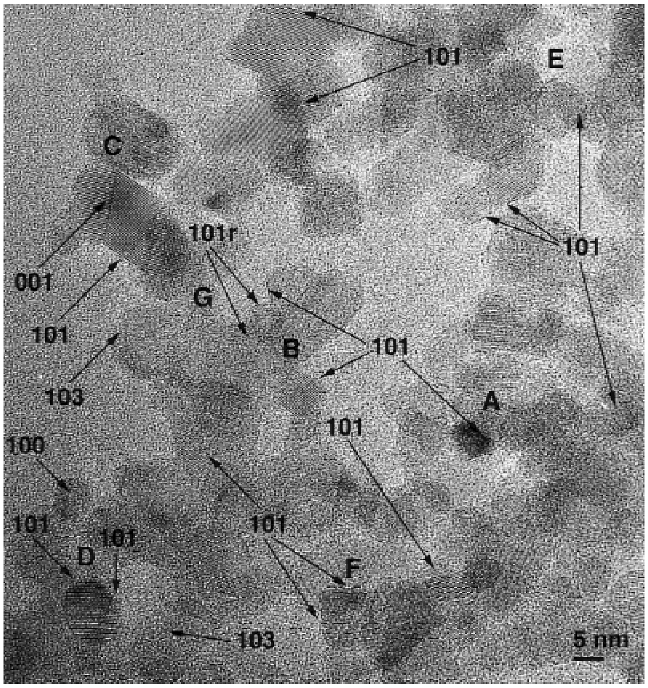

Fig. 3. TEM micrograph of a sample autoclaved at 230°C.

whether the titanium precursor is added dropwise or in one shot. This phenomenon is explained by the very-high water:titanium ratio that is presently used, which renders the kinetic effect of hydrolysis negligible.

Although the precipitate in an acidic environment visually appears to be better dispersed than that which has been hydrolyzed in neutral or basic solution, the three samples appear similar and well dispersed after peptization in acid and hydrothermal growth. This observation is confirmed by the particle-size analysis, which has revealed the presence of aggregates with a median value diameter of 0.15 μm in the three solutions.

BET analysis shows that the three different colloids, after hydrothermal treatment at a temperature of 230°C, have a similar surface area, ~115 ± 2 m^2/g, and the SEM micrographs of the corresponding films are identical. Thus, it can be concluded that neither the precipitation pH nor the alkoxide addition rate has a noticeable influence on the final electrode microstructure.

(B) Role of the Peptization Step: The peptization step was devised to destroy agglomerates that formed during precipitation. The energy that is needed for the deagglomeration was provided by the thermal energy that was supplied during the heating, and the stabilization was ensured electrostatically by the presence of 0.1*M* acid. In fact, the peptization of the colloid should be easier the more the pH value deviates from the isoelectric point (pH of 6.5–7).[13]

Table I shows that substantial growth also occurs during peptization. The surface area decreases from ~297 m^2/g to 165 m^2/g at the end of the peptization, which corresponds to a particle growth from 5.4 nm to 9.4 nm (in average diameter). This decrease in surface area also could be attributed to densification phenomena that are linked to the crystallization of the nanoparticles during peptization. Although the XRD pattern of the as-precipitated powder exhibits some peaks that correspond to anatase (see Fig. 7), the differential thermal analysis (DTA) spectrum of this powder shows the presence of an exothermic peak at ~350°C that can be attributed to crystallization.[8] This peak is absent in the DTA spectrum of the peptized sample, which suggests that crystallization is occurring during peptization. Because the density of amorphous TiO_2 is expected to be significantly lower than that of anatase, the particle growth might not be as important as stated previously.

(C) Influence of Autoclaving Temperature on Primary Particle Growth: The autoclaving step is designed to grow the primary particles further by dissolution–reprecipitation mechanisms that occur under hydrothermal conditions. The BET results (summarized in Table I) clearly indicate that there is a decrease in surface area that can be translated to the primary particles or crystallite growth. SEM investigations confirm this growth (see Fig. 2). TEM investigation (see Fig. 3) shows that all the primary particles are crystalline; the faces are predominantly oriented along the <101> direction.

(D) Influence of Autoclaving Temperature on Aggregation: Particle-size analysis was performed on samples that were autoclaved at different temperatures. The results, which are presented in Fig. 4, reveal that, in parallel to the primary particle growth, an important aggregation occurs. Although the fines are underestimated, because of light scattering, the formation of aggregates (average size of ~0.3 μm) with changes in the temperature is clearly visible.

The autoclaving temperature also has an influence on the pore-size distribution of the final TiO_2 film (see Fig. 5). During the deposition, the concentration of solids in the suspension will increase on drying until the aggregates come into physical contact with each other and form a three-dimensional network. Then, the pore sizes are determined by the aggregate size and shape. The latter is dependent on the aggregation mechanisms that are dictated by the chemical environment. Therefore, for an identical coating procedure, the pore-size distribution in the film will be greatly influenced by the aggregate size in suspension. In fact, we have observed a direct correlation in the present case between the average pore size and the average aggregate size (see Fig. 6). Of course, the pore-size distribution will be influenced by many other processing parameters, such as the amount of binder or the sintering temperature and time. Some of these topics will be discussed in the following subsections.

(E) Influence of Autoclaving Temperature on Rutile Formation: XRD analysis was performed on samples that were autoclaved in 0.1*M* nitric acid solution at different temperatures. The results are presented in Fig. 7. Only the samples that were autoclaved at a temperature of ≥240°C exhibited peaks that corresponded to the rutile phase. Using the Debye–Scherrer relation, we calculated the rutile crystallite size to be ~200 nm in the 250°C sample, which is an order of magnitude larger than the average anatase crystallite size (15 nm). In addition, no progressive growth was observed, regardless of whether the observation was via XRD or SEM. The rutile particles appeared suddenly at a temperature of 240°C and were already an order of magnitude larger than the anatase crystallites. All these observations suggest that the transformation of anatase to rutile proceeded by a cooperative transition that involved some local rearrangements in the anatase aggregates before the rutile transition occurred. This hypothesis of a cooperative transition is supported by the micrographs that are shown in Fig. 8, where clusters of anatase particles are buried inside the larger rutile crystals. Moreover, as we will show later, modification of the titanium alkoxide by acetic acid prevents this aggregation and prevents the formation of the rutile phase, even at a temperature of 250°C; this suggests that, by preventing aggregation of the anatase particles during the hydrothermal step, the formation of rutile is prevented. This observation also confirms the cooperative nature of the transition.

(F) Influence of pH during the Hydrothermal Step: To study the influence of pH during hydrothermal growth on the morphology of the particles, samples that were hydrolyzed in acid have been autoclaved at a temperature of 250°C for 12 h in (i) 0.1*M* nitric acid solution, (ii) ammonia at pH 11, and (iii) 0.1*M* triethylamine at pH 13. SEM micrographs (Fig. 9) and BET results (Table II) both show that the particles were larger under basic conditions than under acidic conditions, which suggests that Ostwald ripening is more important in a basic environment. This observation suggests that the transient species that are formed in a basic environment under hydrothermal conditions are more stable than those which are formed at low pH (acidic conditions). This stability of the intermediate spe-

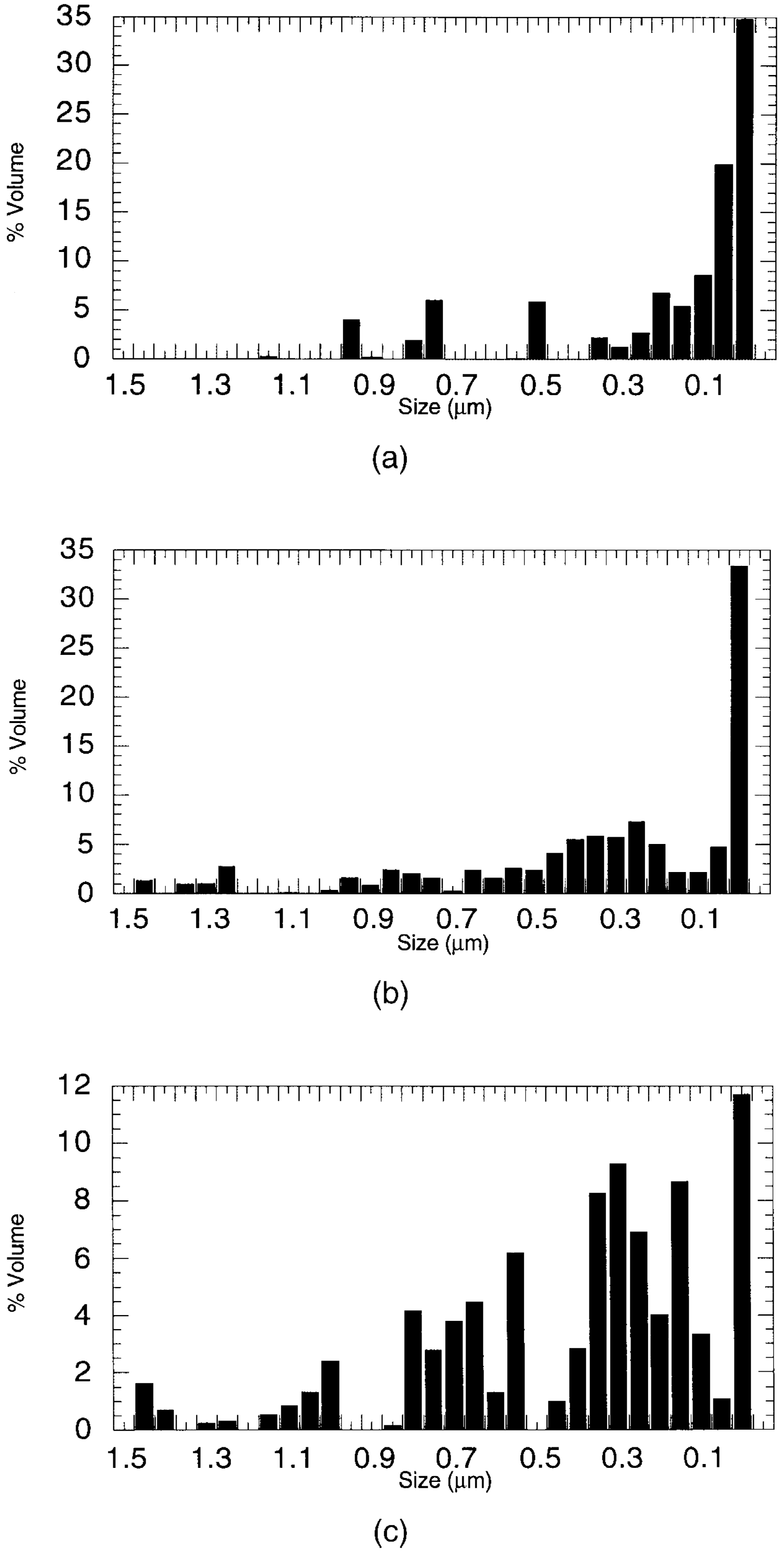

Fig. 4. Particle-size distributions of colloids autoclaved at (a) 210°, (b) 240°, and (c) 250°C.

cies and, therefore, the increase in the solubility of the TiO_2, also could be due to a complexation by the counter ion (NH_4^+ or triethylamine) that stabilizes the anionic species that is formed by dissolution in a manner that is analogous to that which has been observed with sulfate (SO_4^{2-}) or fluoride (F^-) ions.[14] In addition, the redissolution of the TiO_2 increases as the concentration of base increases, in a manner that is similar to what has been observed in hydrothermal growth in acidic media.[15]

(G) Influence of Binder Addition: To study the influence of binder addition on film porosity, different amounts of carbowax (PEG, MW = 20000) were added to a suspension of P25 (Degussa AS, Frankfurt, Germany) in 0.1*M* nitric acid solution. P25 was chosen because of the possibility to produce

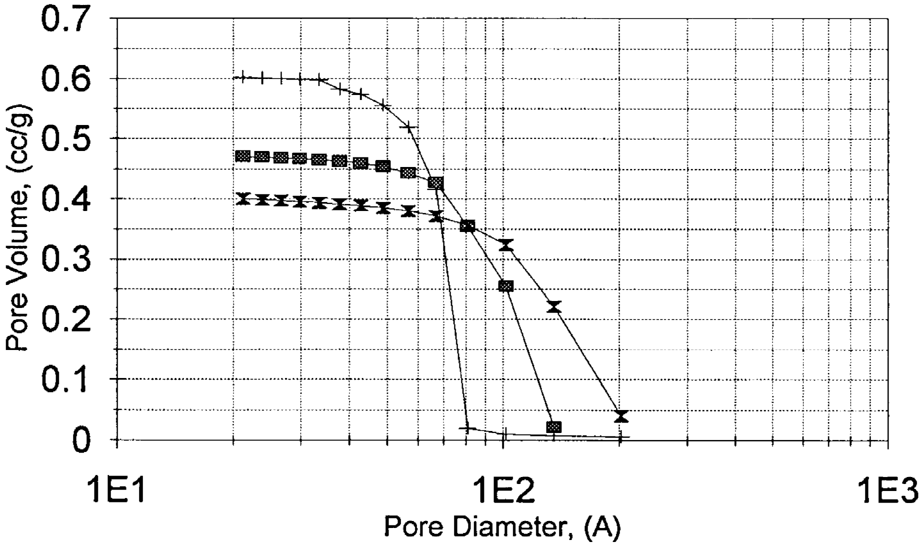

Fig. 5. Cumulative pore-size distributions of films synthesized from colloids autoclaved at (+) 210°, (■) 230°, and (⧗) 250°C.

crack-free films that are 10 μm thick without any binder addition. Pore-size-distribution analysis and total-porosity measurements were performed on the different samples, and the results are presented in Figs. 10 and 11. For the samples that contained 0, 10, and 30 wt% of binder, the average pore size remained centered at 30 nm, although the distribution became broader toward the larger pores. Increasing the amount of carbowax increased the total porosity, as shown in Fig. 11, which suggests that the average pore size was still dependent on the average cluster size, which was constant in the three samples. For the sample that contained 50 wt% of binder, the average pore size increased to 50 nm and the distribution was much broader, with pores as large as 120 nm, which suggests that we are in a region where the morphology of the porous network is not governed by the percolation of the TiO_2 clusters anymore. In fact, a proportion of carbowax of 50% of the weight of TiO_2 represents a binder:TiO_2 volume ratio of 19.

(H) Influence of Sintering: Films were fired at 400°, 450°, 500°, and 550°C at a rate of 5°C/min in air to study the influence of the heat-treatment temperature on the final film morphology. Deformation of our borosilicate glass substrates at 600°C limited our heat treatment to a maximum temperature of 550°C. A decrease in surface area (see Table III) revealed that sintering was occurring, even at these low temperatures; this was confirmed by dilatometry, which showed that pellets that were made by dry pressing the TiO_2 nanoparticles started to shrink in the temperature range of ~350°–400°C. The pore-size measurement that was performed on the films showed that pore coarsening was occurring during sintering (see Fig. 12(a)). The average pore size increased from 15 nm, at a temperature of 400°C, to 20 nm; more specifically, the number of small pores (i.e., <10 nm in size) decreased substantially while, simultaneously, the pore-size distribution expanded toward the larger pores. Stabilization of this pore coarsening was observed after a temperature of 500°C was attained (i.e., the pore-size distribution did not change).

When the films were introduced directly at a temperature of 500°C and fired for times that ranged from 30 min to 5 h, to study the influence of the sintering time on the final film microstructure, a similar phenomena was observed (see Fig.

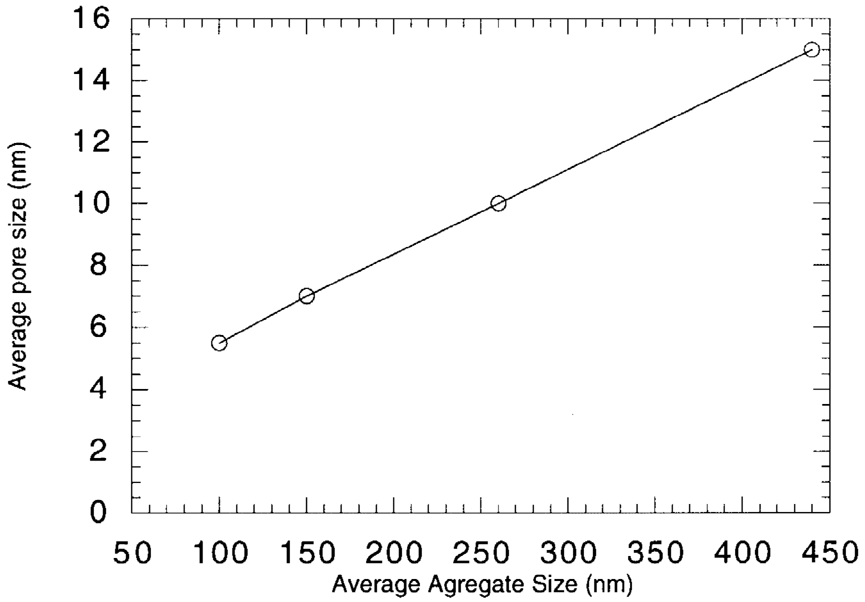

Fig. 6. Average pore size versus average aggregate size for particles processed in 0.1*M* nitric acid.

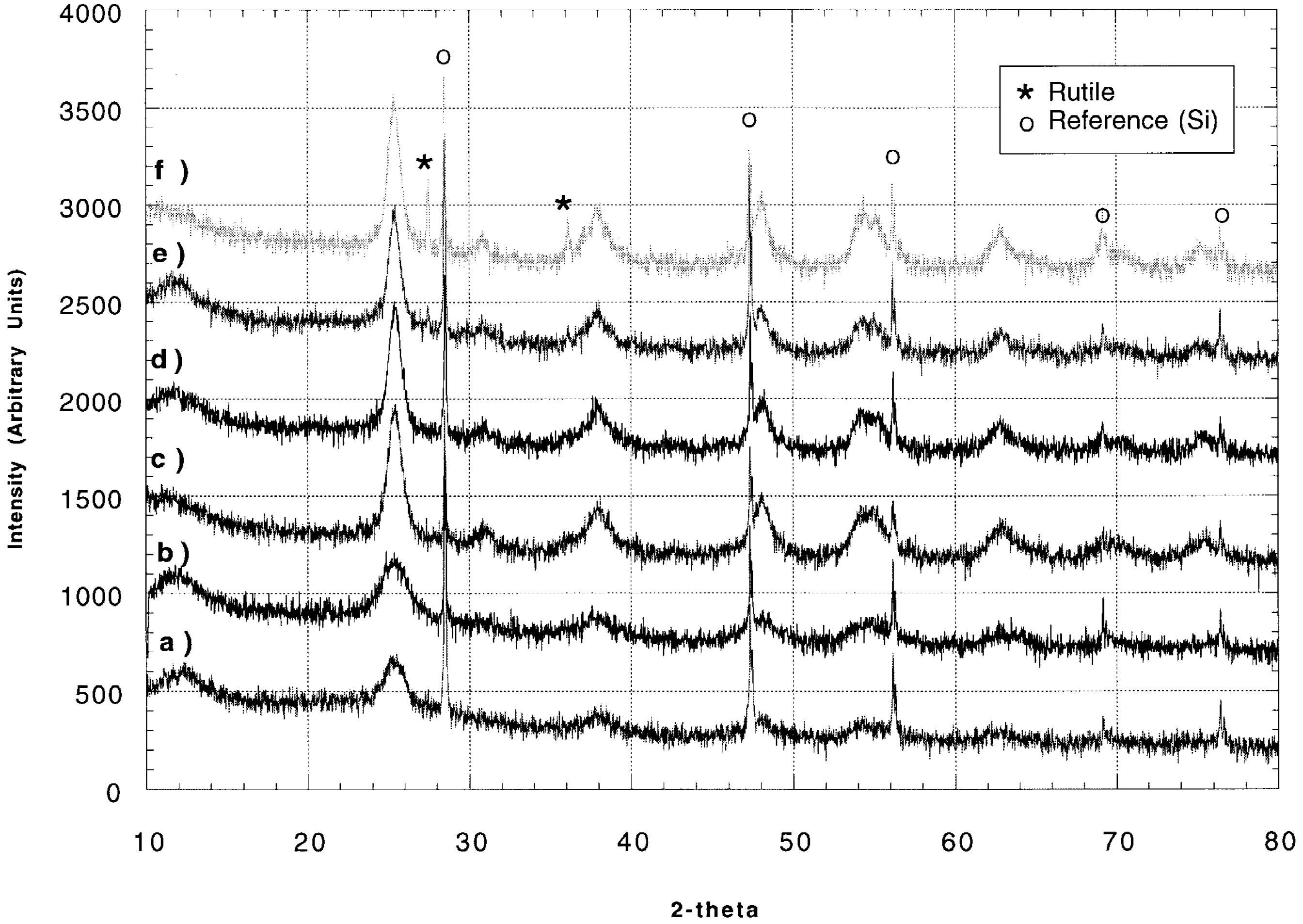

Fig. 7. XRD spectra of the TiO_2 colloid just after precipitation (spectrum ''a''), after peptization (spectrum ''b''), autoclaved at 200°C (spectrum ''c''), autoclaved at 230°C (spectrum ''d''), autoclaved at 240°C (spectrum ''e''), and autoclaved at 250°C (spectrum ''f'') in a 0.1*M* nitric acid solution.

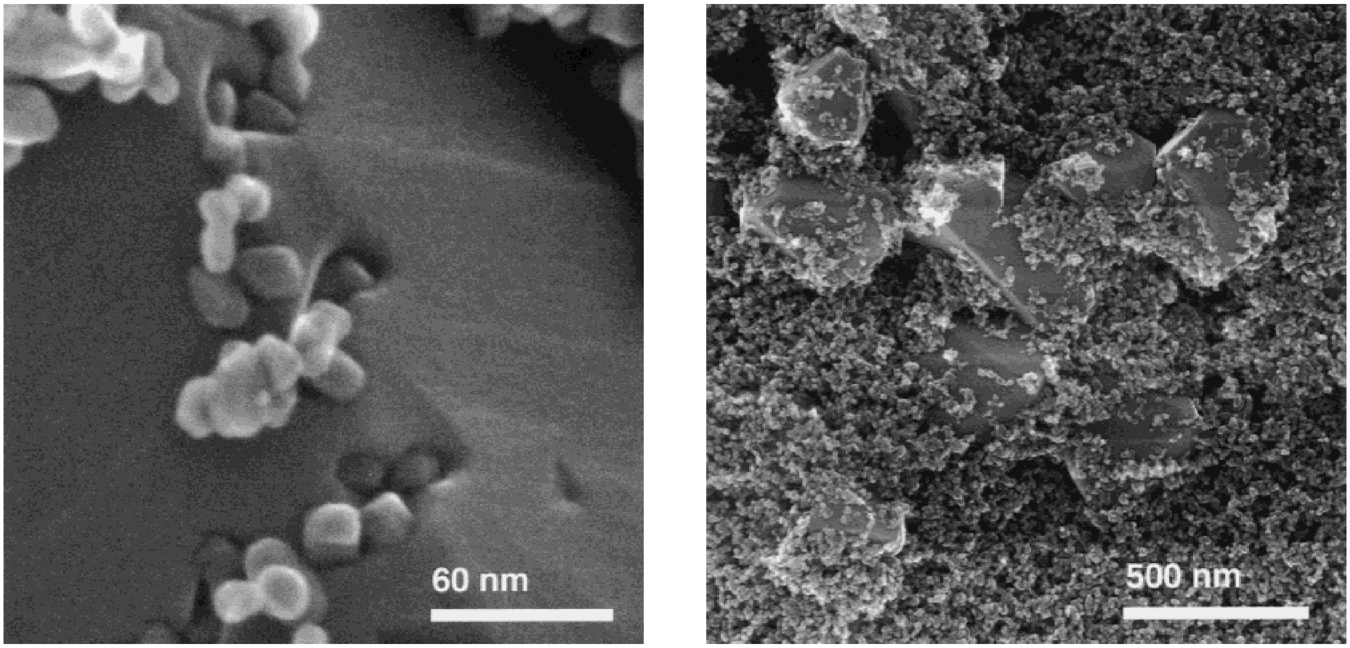

Fig. 8. SEM micrographs of a film synthesized from a colloid autoclaved at 260°C.

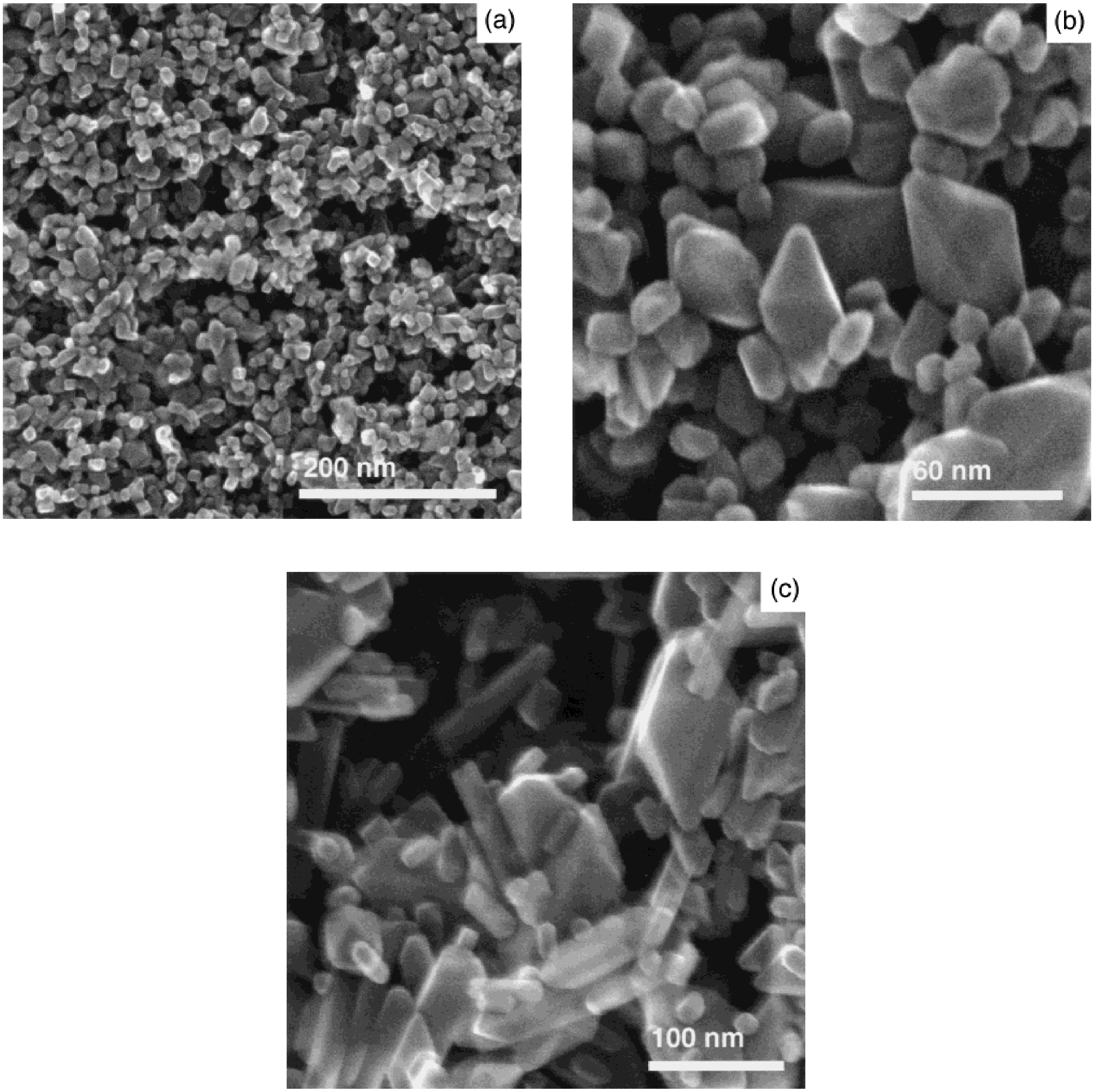

Fig. 9. SEM micrographs of films synthesized from colloid autoclaved at 250°C in (a) a 0.1*M* nitric acid solution (pH 1), (b) a pH 11 ammonia solution, and (c) a 0.1*M* triethylamine solution (pH 13).

12(b)). As the sintering proceeded, pore coarsening occurred simultaneously.

(2) Influence of TiO_2 Electrode Microstructure on the Photovoltaic Properties

(A) Influence of Pore-Size Distribution: To study the influence of the pore-size distribution on the photovoltaic response of the solar cells, two films that have a similar surface area (~55 m^2/g) but different pore-size distributions (see Fig. 13) have been used as photoelectrodes for our solar cells to characterize their photovoltaic properties. Their current–voltage curves have been recorded under 1 Sun and 1/10 Sun. The results are summarized in Table IV. The electrode with the smaller pores exhibits an important nonlinearity (i.e., to be linear, the current at 1 Sun should be larger than the current at 1/10 Sun by a factor of exactly 10). Under reduced illumination

Table II. Surface Area and Average Particle Size for Colloids Peptized in Acid but Autoclaved at 250°C at Different pH Values

Powder	Surface area (m^2/g)	d_{BET}[†] (nm)
In a 0.1*M* solution of nitric acid (pH 1)	108	14.5
In a solution of ammonia (pH 11)	76	20
In a 0.1*M* solution of triethylamine (pH 13)	42	37

[†] Average diameter back-calculated from the surface area, assuming that the particles are spherical.

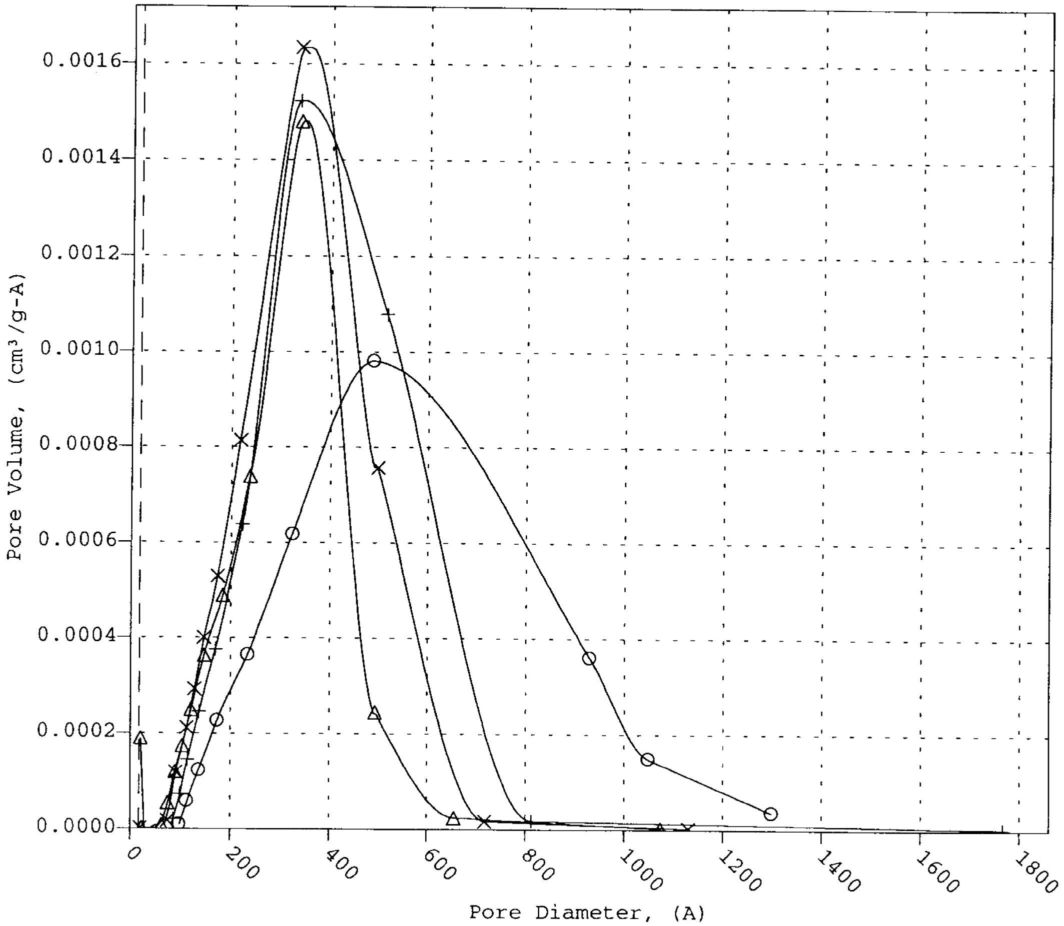

Fig. 10. Influence of binder addition ((△) 0%, (×) 10%, (+) 30%, and (○) 50% binder) on pore-size distribution.

(1/10 Sun), the transport kinetics are fast enough to regenerate (i.e., reduce) the dye; however, under full illumination, ten times more dye molecules are active, and the transport of I^{3-}/I^- ions to and from the counter electrode is not fast enough to fully regenerate the dye molecules. This observation could be explained by the fact that, in pores with a diameter of 4 nm, 3 nm are occupied by the dye molecules (molecular diameter of 15 Å (1.5 nm)) that are adsorbed on the pore walls, which leaves an aperture of only 1 nm for the diffusion of the electrolyte. This distance is very similar to the size of the I^{3-} ion, especially if one considers its solvation shell, and Fick's law of diffusion is not valid anymore. The diffusion kinetics in the

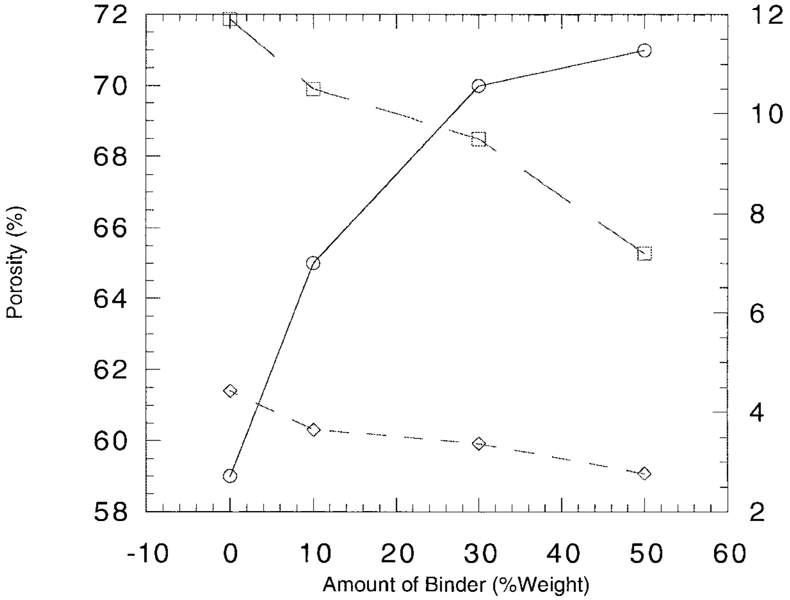

Fig. 11. Influence of binder addition on (○) porosity and photovoltaic properties ((□) I_{SC} at 1 Sun and (◇) yield at 1 Sun).

Table III. Influence of Sintering Conditions on Surface Area of Films

	Surface area (m^2/g) for various sintering temperatures				Surface area (m^2/g) for various sintering times			
Film conditions	400°C	450°C	500°C	550°C	30 min	1 h	2 h	5 h
Sintered by 5°C/min and 30 min	126	104	101	88				
Fired directly at 500°C in air					121	111	103	86

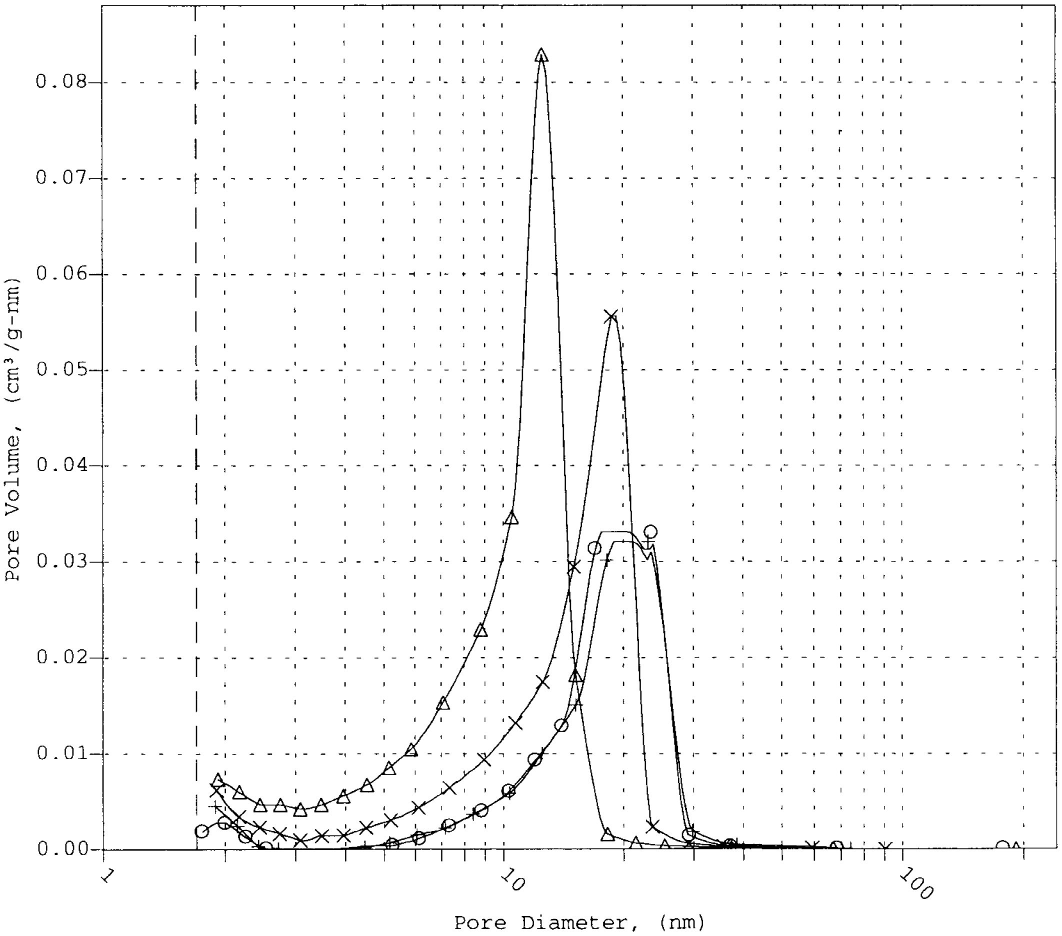

Fig. 12. Influence of sintering temperature ((△) 400°, (×) 450°, (+) 500°, and (○) 600°C) on the pore-size distribution.

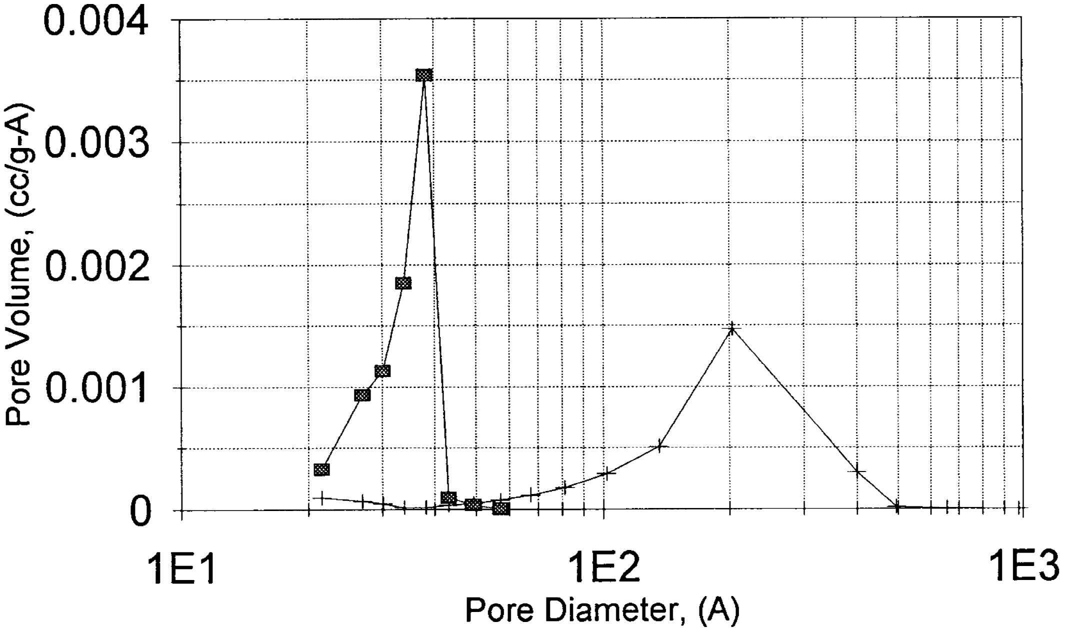

Fig. 13. Pore-size distributions of films synthesized (■) from P25 and (+) from a colloid autoclaved at 230°C in a 0.1*M* triethylamine solution.

Table IV. Comparison of Photovoltaic Properties of Two TiO_2 Electrodes with the Same Surface Area but Different Pore-Size Distributions

	I_{SC} (mA/cm^2)	V_{0C} (mV)	Efficiency (%)
Electrode with average pore size of 4 nm			
1/10 Sun	1.4	550	4.72
1 Sun	9.2	620	3.38
Electrode with average pore size of 20 nm			
1/10 Sun	1.3	560	4.9
1 Sun	12.1	630	5

electrolyte become the limiting step in the current production, which, of course, has a dramatic influence on the efficiency, which decreases from 4.7% to 3.4%. In the sample that has the larger pore size, no nonlinearity is observed and the efficiency is the same at 1/10 Sun or 1 Sun.

Therefore, the presence of small pores slows the diffusion in the electrolyte and, thus, affects the photovoltaic response of the solar cell, especially under high illumination. Of course, other parameters, such as the viscosity of the electrolyte solvent and the concentration of iodine, will affect the transport kinetics.

(B) Influence of Surface Area and Porosity: The current that is produced by the solar cells is directly linked to the number of dye molecules that are adsorbed on the TiO_2 electrode. Therefore, the higher the surface area, the higher the current that is generated by the solar cell; this is one of the key reasons for using TiO_2 nanoparticles.

The porosity of the electrode also drastically influences the photovoltaic properties. In Fig. 14, we have observed that TiO_2 electrodes that have a constant film thickness (~10 μm) and a constant surface area (~55 m^2/g) but an increasing porosity generate less current. This phenomenon is explained by the fact that, when the porosity increases, the mass of TiO_2 per square centimeter of film decreases; thus, the total TiO_2 surface per square centimeter of film decreases. If less surface is available, then there are less dye molecules that are adsorbed per square centimeter of film; thus, the current decreases as the porosity increases. If the current decreases, then the efficiency of the solar cell automatically decreases. In fact, the determining figure of merit for the photo current is the number of dye molecules per unit volume of film, which, in terms of electrode microstructure, is the product of the surface area and the density and can be expressed by the surface area of TiO_2 per unit volume of film.

(3) Role of $TiCl_4$ Post-Treatment

The $TiCl_4$ treatment increases the injection of electrons into the TiO_2 (see Fig. 14) and, thus, the current that is delivered by the solar cell. Two hypotheses can explain this improvement of the injection after treatment: (i) small particles are nucleated on the surface of our electrode and, thus, the surface area and the amount of dye that is adsorbed increases, or (ii) the electron percolation in the TiO_2 mesoporous film is improved.

Table V shows that the $TiCl_4$ treatment decreases the surface area of the films. Therefore, the first hypothesis can be rejected. In addition, the $TiCl_4$ treatment decreases the average pore size (see Fig. 15) and the porosity (see Table V). All this data suggests that the titanium complexes that are present in the $TiCl_4$ solution condense at the interparticle neck. This hypothesis is consistent with the pore-size reduction, the surface-area loss, and the densification that are observed in the films after the $TiCl_4$ treatment. In addition, the increase of the necking between the particles will facilitate the percolation of the electrons from one particle to the other, which will lower the recombination probability and lead to a global increase of the current. More-sophisticated analysis such as femtosecond fluorescence spectroscopy would be needed to prove that the recombination rate is actually affected by this treatment.

(4) Influence of Precursor Chemistry on Film Morphology

It is well known in sol–gel chemistry that the precursor chemistry influences the hydrolysis and the condensation kinetics and, thus, the final material morphology. In the present case, we have attempted two different approaches to control our nanoparticle size and morphology. The first approach consisted of substituting the isopropoxy groups with more-hydrolyzable (ethoxy) groups and less-hydrolyzable (*n*-butoxy) groups. In both cases, the alkoxides are in the form of oligomers, which is contrary to titanium isopropoxide, which is a monomer.[16] The presence of oligomers is known to slow the condensation reactions. The second strategy consisted of substituting one isopropoxy group with a less-hydrolyzable group (i.e., acetate or acetyl acetone). Experiments that were con-

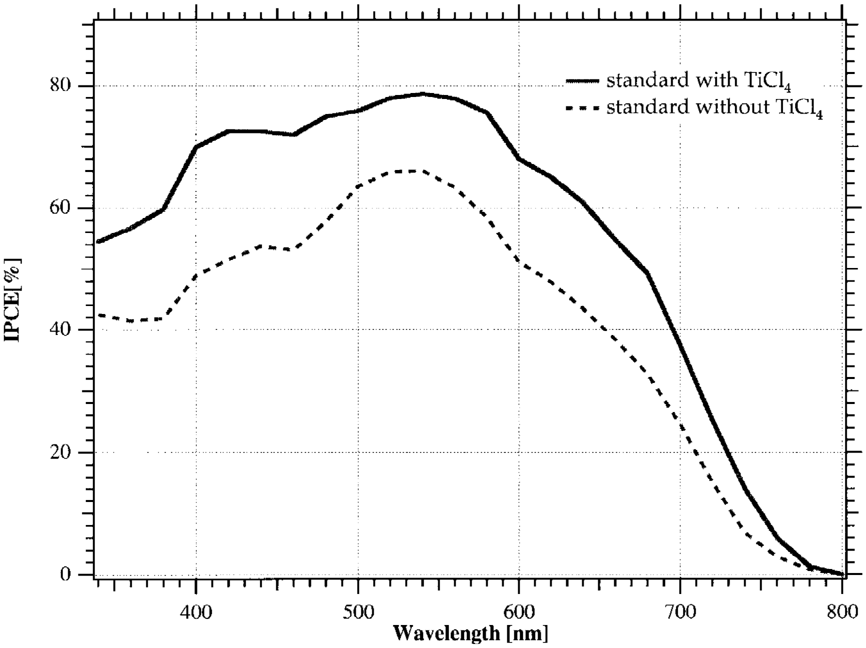

Fig. 14. Action spectra of a standard electrode (—) with and (- - -) without $TiCl_4$.

Table V. Influence of $TiCl_4$ Treatment on Surface Area and Porosity of Different Electrodes

	Surface area (m^2/g)		Porosity (%)	
Electrode	Before treatment	After treatment	Before treatment	After treatment
Colloid 230[†]	125	105	64	60
Standard[‡]	110	97	56	56
P25[§]	55	51	59	53
FD3[¶]	42	36	27	13

[†] Electrode synthesized from a colloid autoclaved at pH 1 and 230°C. [‡] Electrode synthesized from 85% of the previous colloid and 15% of anatase from Fluka Chemical. [§] Electrode synthesized from P25 from Degussa AS. [¶] Electrode synthesized from a colloid autoclaved at pH 13 and 230°C.

ducted by Livage *et al.*[17] showed that the hydrolysis of such modified precursors led to more monodisperse and smaller sols.

The BET results of the corresponding peptized sols are presented in Table VI. Substituting ethoxy or *n*-butoxy groups for the isopropoxy group does increase the surface area moderately. The effect of the substitution on the hydrolysis and the condensation reaction are masked because of the very-high water:alkoxide ratio (i.e., 50 mol of H_2O per titanium atom) that has been used in our synthesis. Modification by acetic acid or acetyl acetone has a drastic effect on the surface area. The effect is more important in the case of the acetyl acetonate modification, because the titanium acetyl acetone (acac-Ti) is not as hydrolyzable as the titanium acetate (CH_3COO-Ti). Unfortunately, the acetyl acetone decomposes during the hydrothermal growth, which leads to a heavily aggregated sol.

Therefore, we will concentrate on the study of the acetic-acid-modified TiO_2. Table VI shows that hydrothermal growth is more important in the modified colloid than that which is observed in the colloid that has been synthesized from titanium isopropoxide; this is due to the fact that the particles are smaller and, therefore, can dissolve more easily under hydrothermal conditions. The smaller the particles, the more pronounced the Ostwald ripening effect. This higher growth rate has been confirmed by SEM (see Fig. 15). Another remarkable feature of this colloid that has been synthesized from the acetic-acid-modified precursor is that it is almost nonaggregated, in comparison with that which has been synthesized from titanium isopropoxide, which suggests that the acetate groups that are located at the surface of the particles act as a dispersing agent and prevent aggregation during the hydrothermal step.

The last characteristic of this colloid (but not the least important) is that the photovoltaic performances of the resulting electrodes are much better than that which has been processed using the classical route (see Fig. 16). More-detailed characterization (e.g., TEM) is underway to determine whether these increased performances are due to the film morphology only or to a different crystallographic orientation of the particle faces, which will enable a better injection.

(5) Influence of Scattering on the Photovoltaic Response of Solar Cells

The electrodes that are prepared using colloids that have been autoclaved at temperatures ≤230°C are fully transparent, and those that have been made from colloids that have been autoclaved above this temperature are translucent or opaque. The electrodes that are synthesized from the particles that have been autoclaved at 250°C give a better photovoltaic response, because of their ability to scatter light. The scattering of light increases the path length of the photons inside the cell and, thus, increases its probability to interact with a dye molecule and inject an electron into the semiconductor; this is especially important for the red light (wavelength of ~700 nm), where our dye is not very efficient. Certain limitations have been encountered with this process temperature: (i) the size distribution of the colloid that has been autoclaved at a temperature of 250°C is difficult to reproduce and (ii) the colloid contains some rutile (up to 30 wt%), which is photoactive at wavelengths of >400 nm and should be avoided, for long-term stability reasons.

To control the number of scattering centers in the layer, a commercial anatase powder (Fluka) that contained large scattering particles was mixed with our synthesized transparent colloid that was autoclaved at a temperature of 230°C. This anatase had a broad particle-size distribution that was centered

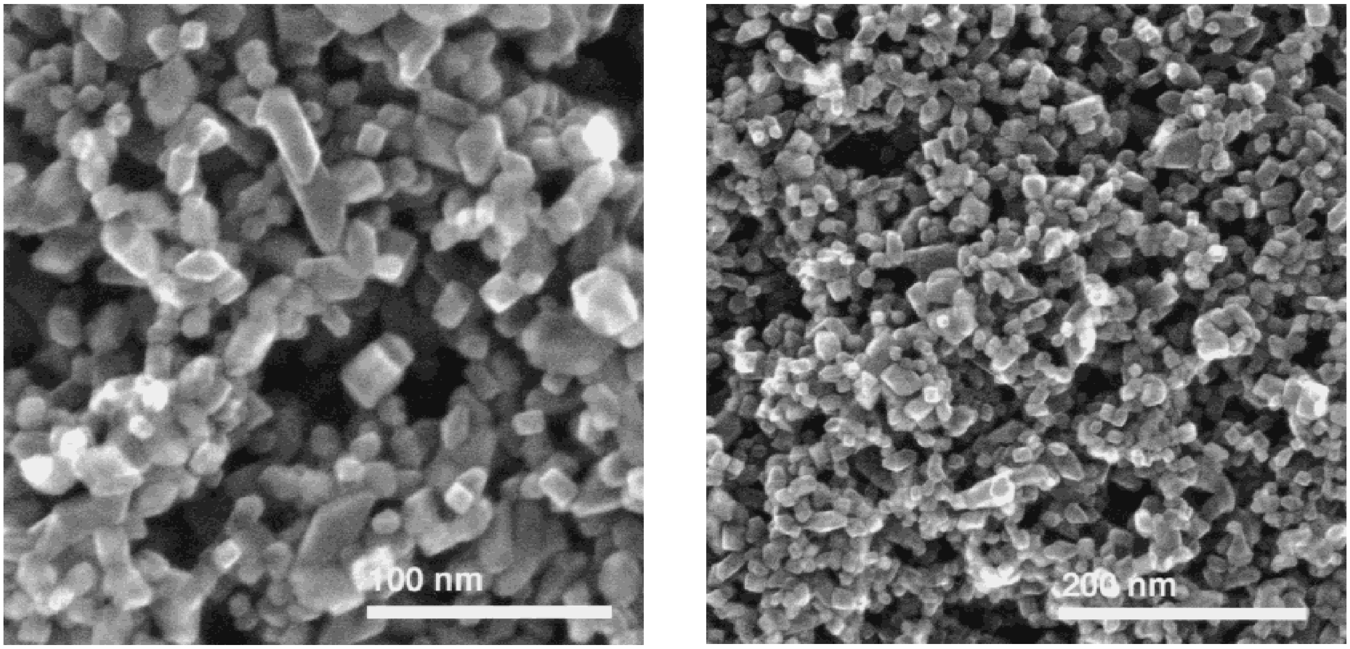

Fig. 15. SEM micrographs of the colloid synthesized from the acetic-acid-modified precursor and autoclaved at 230°C.

Table VI. Influence of Precursor Chemistry on Surface Area and Particle Size of the Corresponding Peptized Sols

Precursor	Surface area (m^2/g)	$d_{BET}^{\dagger}$ (nm)
Titanium isopropoxide	165	9.5
Titanium ethoxide	186	8.4
Titanium butoxide	175	8.9
Titanium isopropoxide modified with acetic acid	217	7.2
Titanium isopropoxide modified with acetyl acetone	293	5.3

†Average diameter back-calculated from the surface area, assuming that the particles are spherical.

at ~300 nm and a surface area of 8 m^2/g. The Fluka particles, although 99% anatase, were coated with a very thin layer of silica (SiO_2) or silicone derivatives; this was discovered by studying the zeta potential evolution, relative to pH. The isoelectric point of the Fluka particles was 2.9 (instead of 6.5–7 for anatase), which corresponded to that of SiO_2 and was latter confirmed by electron spectroscopy for chemical analysis (ESCA). The presence of SiO_2 at the surface of the particles posed two problems. The first problem was that the particles did not sinter at temperatures <1000°C; therefore, the large particles were embedded and held by the nanoparticles that sintered around them (see Fig. 17). No films with a decent mechanical resistance could be obtained with $\geq$30 wt% Fluka particles. At 30 wt%, we reach the percolation threshold and the large particles are coming into contact with each other; because they do not sinter, the mechanical stability of the layer is lost. The second consequence of the presence of a SiO_2 layer at the surface was that these particles were inactive, with respect to the injection, which explains why, in addition to the fact that more Fluka particles lower the surface area of the film, the optimum composition was 85% of nanocrystalline particles that had been autoclaved at a temperature of 230°C and 15% Fluka particles.

A comparison of specular and diffuse transmissions between a solar cell with a transparent electrode and a solar cell that incorporates scattering centers (see Fig. 18) clearly illustrates the effect of the scattering particles. Increased adsorption in the sample that contains the scattering particles leads to better injection, especially in the region of >600 nm. To understand the influence of other important parameters, such as the size distribution of the scattering particles and the thickness of the layer, we are currently developing a model for the optical properties of the solar cell.

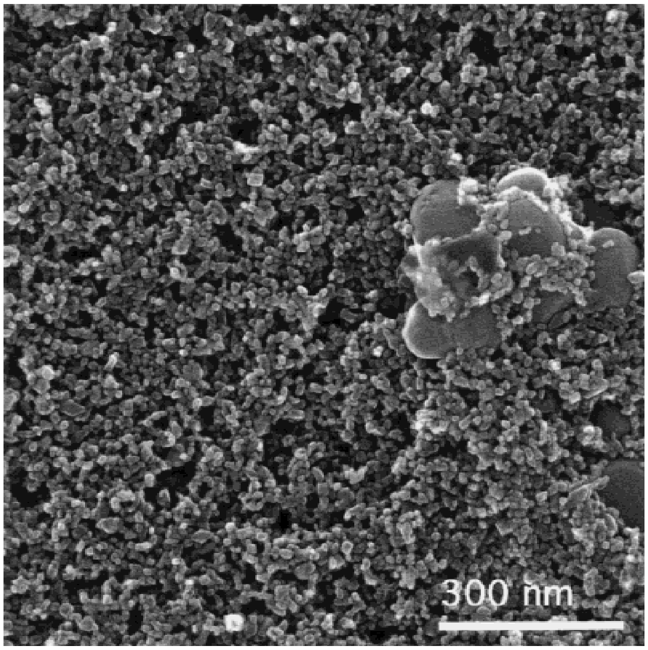

Fig. 17. SEM micrograph of a film containing 15 wt% anatase from Fluka Chemical.

IV. Conclusions

We have shown that the TiO_2 electrode microstructure can be controlled by controlling different processing steps during the synthesis of the nanoparticles. The size of the primary particles and the surface area are controlled by parameters such as the temperature and pH during the hydrothermal step. The average pore size is dependent on the average size of the ag-

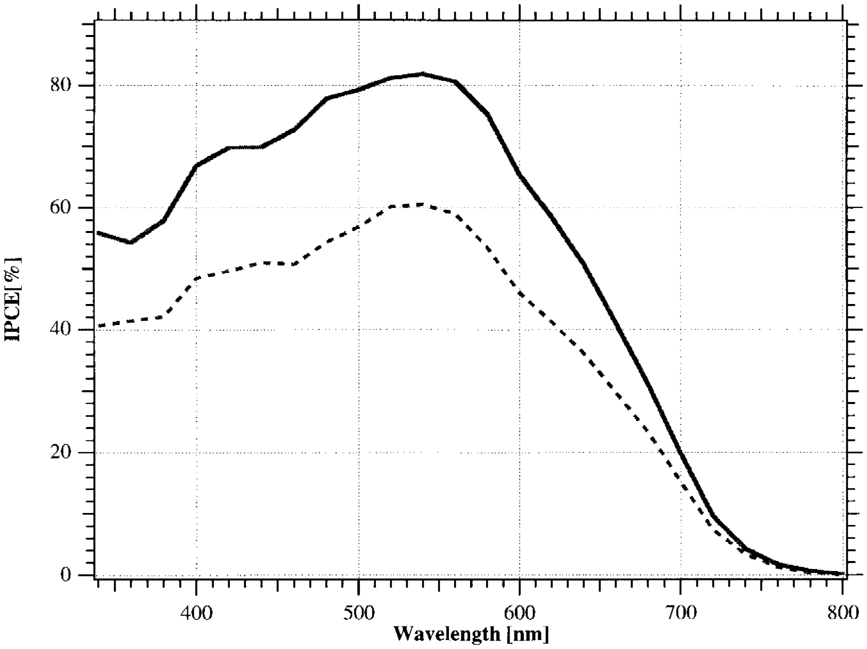

Fig. 16. Action spectra of the electrodes processed from (- - -) isopropoxy-modified and (—) acetic-acid-modified precursors.

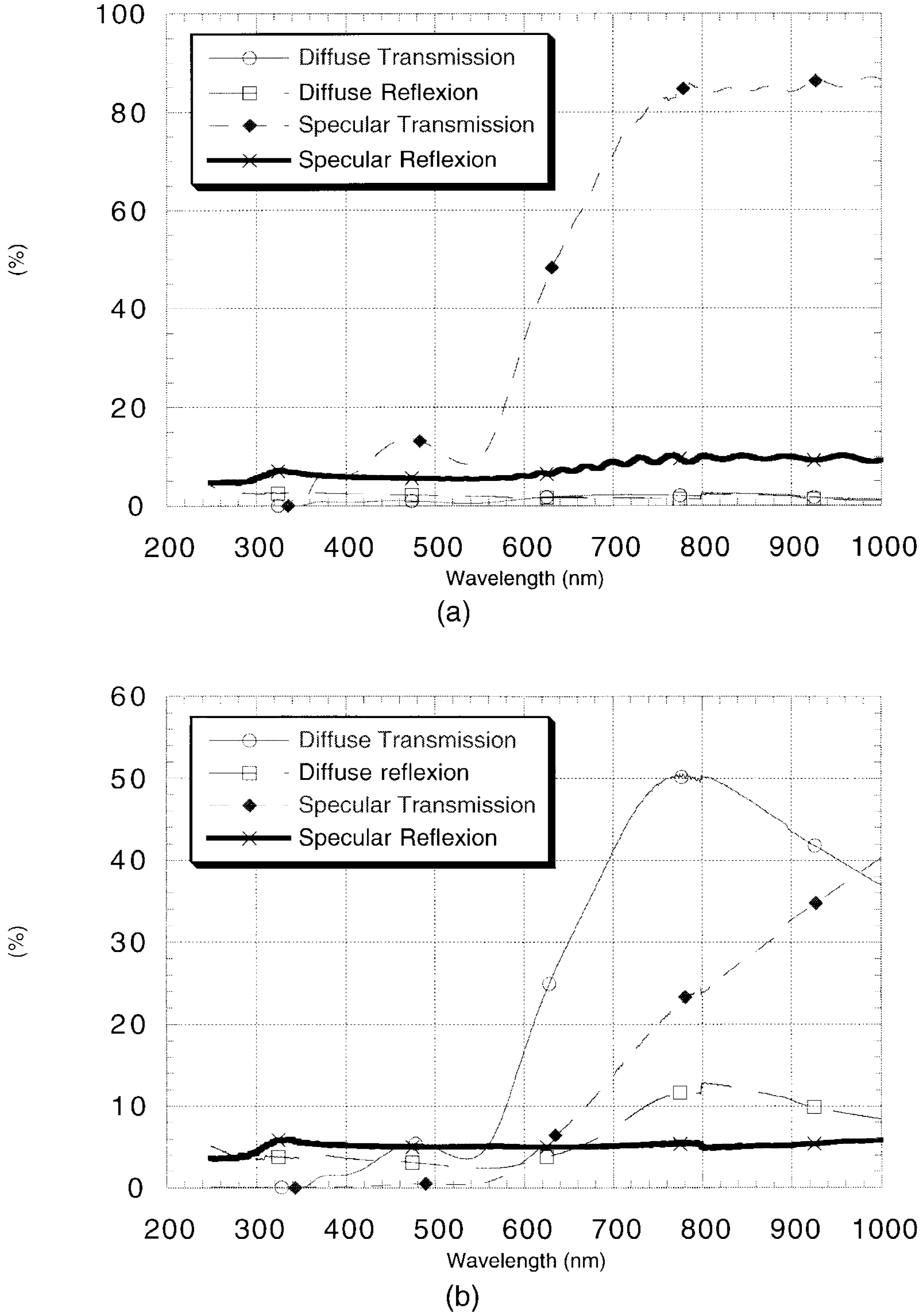

Fig. 18. UV–VIS characterization of two solar cells with (a) a transparent photoelectrode (colloid 230°C) and (b) a scattering photoelectrode (with 15% Fluka particles).

gregates that are formed during the peptization. The pore-size distribution can be altered by adding various amounts of binder or by varying the sintering temperature and time, thus promoting pore coarsening. The formation of rutile during the hydrothermal step can be avoided by maintaining a temperature of <240°C or by preventing aggregation by modifying the precursors with acetic acid or some polymeric dispersing agent, such as poly(acrylic acid) (PAA).

By controlling the pore-size distribution, we can ensure a good diffusion of the electrolyte and, therefore, increase the linearity and fill factor of the cell. If the pores are too small (i.e., ≤4 nm), a degradation in the performance of the solar cell is observed. By controlling the density and the surface area of the nanocrystalline film, we can control the amount of dye that is adsorbed in the electrode. This quantity is directly linked to the electron injection and the current that is produced by the corresponding solar cell. The current can be further enhanced by treating the TiO_2 electrode with $TiCl_4$, which results in interparticle neck growth and facilitates the electron percolation through the TiO_2.

The addition of larger particles (300–400 nm) to the nanoparticles increases the scattering of the film and increases the adsorption in the red portion of the spectrum, which increases both the injection, especially in the wavelength region of >600 nm, and the current that is delivered by the solar cell. Control of the scattering also is critical for some applications where transparency is required (i.e., active window).

Finally, the choice of titanium precursors has a substantial effect on both the crystallite size and the electrode microstructure and, consequently, the final photovoltaic properties. By modifying the titanium isopropoxide with acetic acid, we modify the condensation reaction, thus producing smaller particles; this results, after hydrothermal treatment, in the production of larger crystallites (compared with the pure isopropoxide), which are very lightly aggregated. The aggregation is prevented by the presence of isopropoxy groups at the surface. Although the reasons are not yet fully elucidated, the modified precursor leads to electrodes with improved photovoltaic performances. We hope that, by using this type of molecular approach, we can further improve our photoelectrodes and ultimately break the 10% efficiency barrier, which is needed for high-power applications.

Acknowledgments: The authors would like to thank their coworker, Conradin Von Planta, for fruitful discussions and technical help for the photovoltaic measurements and Dr. Paul Bowen and Professor Heinrich Hoffman from the Powder Technology Laboratory at EPFL for providing access to their powder-characterization equipment, as well as for stimulating discussions. The authors are indebted to R. Wessicken for the help in recording and interpreting the high-resolution transmission electron microscopy (HRTEM) patterns.

References

[1] A. P. Alivistos, ‘‘Semiconductor Nanocrystals,’’ *MRS Bull.,* **20** [3] 23–32 (1995).

[2] J. C. Parker and R. W. Siegel, ‘‘Optical Determination of the Oxygen Stoichiometry of Nanophase Metal Oxide Materials,’’ *Nanostruct. Mater.,* **1**, 53–57 (1992).

[3] J. S. Foresi and T. D. Moustakas, ‘‘Piezo-resistance and Quantum Confinement in Microcrystalline Silicon’’; pp. 77–82 in *Light Emission from Silicon,* Materials Research Society Symposium Proceedings, Vol. 256. Edited by S. S. Iyer, R. T. Collins, and L. T. Canham. Materials Research Society, Pittsburgh, PA, 1992.

[4] T. G. Nieh, J. Wadsworth, and F. Wakai, ‘‘Recent Advances in Superplastic Ceramics and Ceramic Composites,’’ *Int. Mater. Rev.,* **36**, 146–61 (1991).

[5] M. M. Boutz, R. J. Olde Scholtenhuis, A. J. Winnubst, and A. J. Burggraaf, ‘‘Preparation, Microstructural Control and Superplasticity of Nanostructured Yttria Stabilized Tetragonal Zirconia Ceramics’’; pp. 75–86 in *Nanoceramics,* British Ceramics Proceedings, Vol. 51. R. Freer, London, U.K., 1993.

[6] Q. Xu and M. A. Anderson, ‘‘Sol–Gel Route to Synthesis of Microporous Ceramic Membranes: Preparation and Characterization of Micropourous TiO_2 and ZrO_2 Xerogels,’’ *J. Am. Ceram. Soc.,* **77** [7] 1939–45 (1994).

[7] A. Hagfeldt, N. Vlachopoulos, and M. Graetzel, ‘‘Fast Electrochromic Switching in Nanocrystalline Oxide Semiconductor Films,’’ *J. Electrochem. Soc.,* **141** [7] 82–84 (1994).

[8] B. O’Reagan and M. Graetzel, ‘‘A Low Cost, High Efficiency Solar Cells Based on Dye Sensitized Colloidal TiO_2 Films,’’ *Nature* (*London*), **353**, 737–39 (1991).

[9] M. K. Nazeeruddin, A. Kay, I. Rodicio, R. Humphry-Baker, E. Müller, P. Liska, N. Vlachopoulos, and M. Graetzel, ‘‘Conversion of Light to Electricity by Charge-Transfer Sensitizers on Nanocrystalline TiO_2 Electrodes,’’ *J. Am. Chem. Soc.,* **115**, 6382–90 (1993).

[10] J. Livage, ‘‘Synthesis, Structure and Applications of TiO_2 Gels’’; pp. 717–23 in *Better Ceramics Through Chemistry II,* Materials Research Society Symposium Proceedings, Vol. 73. Edited by C. J. Brinker, D. E. Clark, and D. R. Ulrich. Materials Research Society, Pittsburgh, PA, 1986.

[11] P. Bonhôte, A.-P. Dias, N. Papageorgiou, K. Kalyanasundaram, and M. Grätzel, ‘‘Hydrophobic, Highly Conductive, Ambient-Temperature Molten Salts,’’ *Inorg. Chem.,* **35**, 1168–78 (1996).

[12] C. Von Planta, ‘‘Photo-electrical Characterization of Dye Sensitized Nanocrystalline Cells’’; Ph.D. Dissertation. Swiss Federal Institute of Technology, Lausanne, Switzerland, 1996.

[13] P. McFayden and D. Fairhurst, ‘‘Zeta Potentials of Nanoceramic Materials’’; see Ref. 5, pp. 175–85.

[14] J.-P. Jolivet, *De la Solution à l’Oxide;* pp. 193–95. Intereditions/CNRS, Paris, France, 1994.

[15] J.-P. Jolivet, *ibid,* pp. 99–100.

[16] G. W. Scherer and C. J. Brinker, *Sol–Gel Science;* pp. 43–49. Academic Press, New York, 1990.

[17] C. Sanchez, F. Babonneau, S. Doeuff, and A. Leaustic, ‘‘Chemical Modifications of Titanium Precursors’’; pp. 77–87 in *Ceramic Ultrastructure and Processing.* Wiley, New York, 1988. □